THESIS FOR THE DEGREE OF LICENTIATE OF ENGINEERING

Catalytic Methane Oxidation for Emission Control and Fuel Liquefaction

XUETING WANG

CHALMERS

Department of Chemistry and Chemical Engineering
Division of Applied Surface Chemistry
Competence Centre of Catalysis
CHALMERS UNIVERSITY OF TECHNOLOGY
Gothenburg, Sweden 2017

Catalytic Methane Oxidation for Emission Control and Fuel Liquefaction
XUETING WANG

Licentiatuppsatser vid Institutionen för kemi och kemiteknik
Chalmers tekniska högskola
Nr 2017:12

Department of Applied Chemistry
Competence Centre for Catalysis
Chalmers University of Technology
SE-412 96 Gothenburg
Telephone +46 31 772 1000

Typeset in LaTeX
Printed by Chalmers Reproservice
Gothenburg, Sweden 2016

Catalytic Methane Oxidation for Emission Control and Fuel Liquefaction

XUETING WANG
Department of Chemistry and Chemical Engineering
Chalmers University of Technology

Abstract

This thesis conceptualises fundamental structural understanding of alumina supported Pd-Pt catalysts during complete oxidation of methane and active sites in copper exchanged zeolites for direct conversion of methane to methanol. Model catalysts were prepared by wet-chemical methods and studied during transient conditions using chemical flow reactors and *in situ/operando* spectroscopic (FTIRS and XAS) techniques.

Preparation of Pd-Pt/alumina catalysts requires high calcination temperatures (800 °C) for alloyed nanoparticles to form when in presence of air. Although alloying is made primarily for increased durability, alloyed Pd-Pt shows slightly higher activity for complete methane oxidation. Reversible changes in the structure and chemical state of the nanoparticles occur upon switching between net-oxidizing and net-reducing feed compositions. Under oxidizing conditions Pd segregates to the particle surface and oxidizes forming PdO leaving Pt in a reduced state underneath, while under reducing conditions regions with metallic Pd and Pd-Pt alloys were observed at the surface.

Stoichiometric amounts of methanol can be produced by partial oxidation of methane over isolated Cu ions but likely not over Cu particles employing a sequence where the catalyst is first activated by oxidation at high temperature then exposed to methane at lower temperature followed by addition of water vapour to extract the methanol product from the catalyst. The dynamic interaction between methanol and Cu-ZSM-5 was studied by temperature programmed desorption of methanol using *in situ* DRFITS. Isolated Cu ions at the ion exchange positions in ZSM-5 interact with methanol and its derivatives within a broader temperature range compared to H-ZSM-5, and are responsible for unwanted furthure oxidation of methanol at elevated temperature. Furthermore, methoxy groups seems to interact strongly with ZSM-5, which explains the need for a proton extraction procedure for zeolite-based systems.

Keywords: methane activation; methanol desorption; Pd-Pt nanoparticles; Cu-ZSM-5; temperature programmed desorption; *operando* IR and X-ray absorption spectroscopy.

List of Publications

This thesis is based on the following appended papers:

I. Study of Methane Oxidation over Alumina Supported Pd-Pt Catalysts Using *operando* DRIFTS/MS and *in situ* XAS Techniques
N. M. Martin, J. Nilsson, M. Skoglundh, E. C. Adams, X. Wang, G. Smedler, A. Raj, D. Thompsett, G. Agostini, S. Carlson, K. Norén, and P.-A. Carlsson
Catal. Struct. React., **3** (2017), 24-32

II. Characterization of Surface Structure and Oxidation/Reduction Behavior of Pd-Pt/Al_2O_3 Model Catalysts
N. M. Martin, J. Nilsson, M. Skoglundh, E. C. Adams, X. Wang, P. Velin, G. Smedler, A. Raj, D. Thompsett, H. H. Brongersma, T. Grehl, G. Agostini, O. Mathon, S. Carlson, K. Norén, F. J. Martinez-Casado, Z. Matej, O. Balmes and P.-A. Carlsson
J. Phys. Chem. C, **120** (2016), 28009-28020

III. Characterization of Methanol Desorption from Cu-ZSM-5 by *in situ* Infrared Spectroscopy and First-principles Calculations
X. Wang, A. A. Arvidsson, N. M. Martin, J. Nilsson, S. Carlson, J. Gustafson, M. Skoglundh, A. Hellman and P.-A. Carlsson
In manuscript

IV. Direct Methane Oxidation to Methanol: Activity over Isolated Cu Ions and Cu Particles
X. Wang, N. M. Martin, J. Nilsson, M. Skoglundh, J. Gustafson, S. Carlsson, and P.-A. Carlsson
In manuscript

My Contributions to the Publications

Paper I

I planned and participated in the XAS measurements in MAX IV Laboratory, and co-authored the manuscript.

Paper II

I planned and participated in the XAS measurements in MAX IV Laboratory, and co-authored the manuscript.

Paper III

I prepared the catalysts, performed all experimental work and data analysis, interpreted the results with my co-authors, and wrote the first draft of the manuscript

Paper IV

I prepared the catalysts, performed all experimental work and data analysis, interpreted the results with my co-authors, and wrote the first draft of the manuscript

CONTENTS

CHAPTER 1

INTRODUCTION

Methane consists of one carbon and four hydrogen atoms, *i.e.*, CH_4, and is the simplest molecule among the saturated hydrocarbons (the alkanes). It is the main component in natural gas, which presently attracts much attention as an abundant source of energy [1]. Thanks to the low carbon to hydrogen ratio, more useful energy per formed carbon dioxide is delivered upon combustion as compared to, for example, other hydrocarbon-based fuels [2]. As a vehicle fuel it has many advantages although it is not free from problems. Methane is a strong green house gas and slipped methane from the engine combustion must be carefully controlled [3]. With the rapid growth of produced natural gas powered engines, suitable measures need to be adopted as to abate methane emissions. Despite the many efforts that have been devoted to gas engine design and operation strategies for minimal engine out methane emissions, exhaust aftertreatment systems with oxidation catalysts are needed for complete oxidation of unburnt methane [4]. Furthermore, natural gas engines that operate in oxygen excess (lean conditions) have rather low exhaust gas temperature (below 500 °C) [5]. This brings an extra challenge into the catalyst design as catalyst that are active at low temperatures are needed. For this purpose materials such as supported Pd and/or Pt catalysts have been used so far [6].

Another way to utilize the energy in methane is by converting it to another chemical, preferably a liquid. Methanol is one choice that presently attracts many researchers interests [7,8]. This approach benefits both energy transportation and storage as well as eliminates methane emissions. Industrially, converting methane to methanol is a two-

step reaction process where methane is first partially oxidized to syngas (CO and H_2) at high temperature and subsequently converted to methanol over a $Cu/ZnO/Al_2O_3$ catalyst at high pressure. The overall process, however, is energy intensive and thus costly. In some cases it may also be atomically uneconomic due to parasitic total CH_4 oxidation to CO_2 and H_2O. Therefore, direct conversion of methane to methanol (DCMM) at low temperature and ambient pressure is a desired atom economic alternative with potential low energy consumption.

This work treats on the one hand the complete oxidation of methane for emission control in natural gas powdered vehicles and on the other hand the direct conversion of methane to methanol as an energy carrier and chemical feedstock. Both topics have in common that methane should be activated for further oxidation at relatively low temperatures and ambient pressure. As methane has low reactivity due to its four symmetric non-polar C-H bonds and low sticking probability even on the most active catalytic surfaces, activation of the first C-H bond is a key-step for further reactions. Despite the similarity of the two topics, DCMM faces more challenges as controlled oxidation is required for methanol production.

1.1 Objectives

The present thesis have two main aims. The first is to understand how the calcination conditions and oxidative/reductive treatments determine the surface composition and alloy formation of alumina supported Pd-Pt model catalysts, and how transient conditions influence the activity for complete methane oxidation. The second is to understand the site requirement for partial oxidation of methane to methanol over Cu-exchanged zeolites and the interactions between the methanol product and the Cu-ZSM-5 catalyst, which is one important aspect for the targeted selectivity.

CHAPTER 2
BACKGROUND

2.1 Complete oxidation of methane for emission control

2.1.1 Catalytic materials

Supported noble metal catalysts

Among the catalysts used for complete methane oxidation, alumina supported Pd catalysts have shown highest activity for low-temperature methane oxidation [9]. The active phase in Pd/Al_2O_3 under lean (oxidizing) conditions has been identified as oxidised Pd particles. Although a precise structure have not yet been reported, if at all it exists, it is likely so that under-coordinated Pd atoms in the oxide constitute highly active sites for methane dissociation. For example, a recent study on model surfaces shows that the PdO(101) facet of bulk palladium oxide has a particularly high activity for methane oxidation thanks to under-coordinated surface atoms [10]. Despite the high activity of Pd/Al_2O_3 catalysts further improvements are needed to meet the present and upcoming needs. For example Pd catalysts can be strongly deactivated by sulfur poisoning [11] and are sensitive to water. The latter is an inevitable exhaust component especially in nature gas fuelled vehicles. On the contrary, alumina supported Pt catalysts are less sensitive to sulfur, in fact the methane oxidation activity can be promoted by addition of SO_2 [12], but unfortunately those exhibit suppressed activity in lean environments when surface PtO is present [13, 14]. Increased activity, however, can be achieved over Pt/Al_2O_3 by employing transient conditions, *i.e.*, deliberate switching between lean and

rich (reducing) conditions [14–16].

Supported Pd-Pt catalysts

Compared with monometallic catalysts, the supported bimetallic Pd-Pt catalysts exhibit improved activity for complete methane oxidation at low temperatures [17–20]. Moreover, higher resistance towards sintering [20, 21], water poisoning [22] and sulfur poisoning during rich conditions [23] have been observed over alumina supported Pd-Pt catalysts. The Pt/Pd ratio, however, is an important factor for the catalyst performance. Only small amount of Pt addition is needed for enhancing the activity, while high Pt/Pd ratio can suppress the reaction [24, 25]. Additionally, redistribution and interaction of Pd and Pt have been observed after certain treatment conditions [18, 19, 21, 22], which may be the reason for higher catalytic activity over time.

2.1.2 Conditions for automotive catalysts

As automobile catalysts always experience dynamic reaction conditions, *i.e.* alternations between lean and rich compositions, changes may occur to the catalyst structure and chemical state. Such changes may introduce considerable effects on catalytic activity. For example, the promoting effect of Pt in supported Pd-Pt catalysts for lean conditions may be different when alternating conditions is used. It is thus important to understand on the fundamental level how alloyed Pd-Pt nanoparticles respond to gas composition changes and how these changes in turn impact the catalytic activity for methane oxidation. To bring such knowledge the changes taking place in the catalyst need to be tracked under reaction conditions and correlated to the catalytic activity.

2.2 Partial oxidation of methane to methanol for methane liquefaction

Although DCMM is a preferable route for methane partial oxidation to methanol thanks to high atom economy and potentially low energy consumption, the dilemma, nevertheless, is that activation of methane over heterogeneous catalysts requires high temperature such that formed reaction intermediates easily may undergo further unwanted oxidation reactions. Therefore, the main challenge for DCMM concerns how to achieve

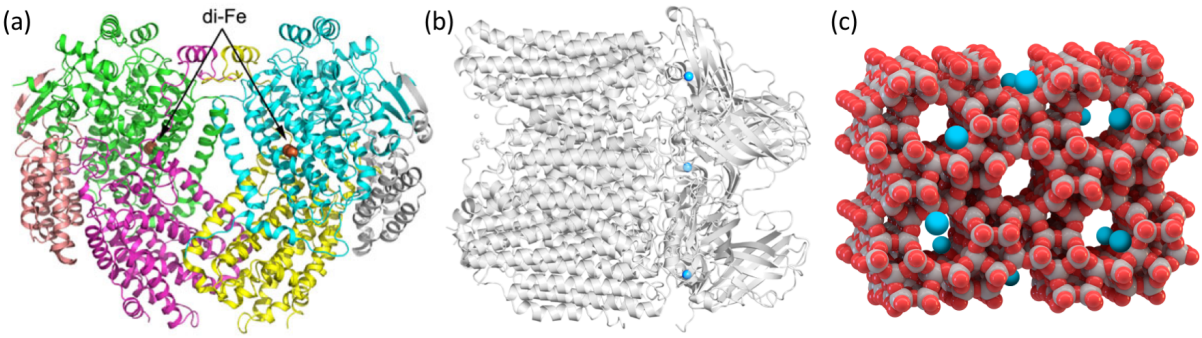

Figure 2.1: Models of structures for catalyzing DCMM; a comparison between enzymes and heterogeneous catalyst. (a) Crystal structure of soluble MMO from Methylococcus capsulatus adapted from [26]; the di-iron centres are shown as spheres. (b) Crystal structure of particulate MMO from Methylocystis adapted from [28]; the copper centres are highlighted in blue. (c) Structure model for Cu-ZSM-5 recreated from [29]; the copper centres are highlighted in blue.

reasonable activity at low temperatures as to obtain the desired selectivity. Conceptually, one may glance at nature and get inspired by the functions in natural enzymes.

Methane monooxygenase (MMO) is a group of enzymes that can selectively oxidize methane to methanol under mild conditions. The active site is a di-iron centre in soluble MMO [26] and a copper centre in particulate MMO [27] in both cases with a ligand environment formed by surrounding peptides, as shown in Figure 2.1a and b. By designing catalysts with active sites that mimic the metal centre as well as the surrounding structure of the metal centre in MMO, high selectivity for methanol may be achieved at low temperature and ambient pressure. Inspired by the structure of MMO, researchers have synthesized and tested various metal-exchanged zeolites. An example is shown in Figure 2.1c schematically presenting the dicopper active sites surrounded by porous zeolite framework.

Depending on the type of oxidant, DCMM over metal-exchanged zeolites can be carried out in either liquid phase or gas phase. For liquid phase DCMM, H_2O_2 is used as oxidant with the reaction temperature kept at 50 °C [30, 31]. For gas phase DCMM, oxidants such as N_2O, NO or O_2 are commonly employed. The usual approach of gas phase DCMM relies on three sequential steps namely i) catalyst activation: creation of active sites by treatment with oxidants at elevated temperature; ii) reaction: the catalyst is cooled down to the reaction temperature and brought into contact with methane;

iii) methanol extraction: by use of water, ethanol or some other protic solvent methanol is extracted as a product [32–47]. Recent studies, however, are more focused on carrying out DCMM isothermally [48–50] or with constant gas feed composition [49] for realising a true catalytic cycle.

Alternatively, to conventional heterogeneous catalysis, research on DCMM have also been carried out using photocatalysis [51–53], Fe-O embedded graphene [54] and by using dielectric barrier discharge [55–57]. This work, however, will be focused on Cu-exchanged zeolites.

2.2.1 Catalytic materials for gas phase DCMM

Copper-exchanged zeolites

Since the observation of DCMM over copper-exchanged zeolites, intensive work has been devoted to, on the one hand, identifying the catalytically active site and, on the other hand, completing the catalytic cycle. For DCMM over Cu-ZSM-5, an absorption band at 22700 cm^{-1} in the UV-visible spectral region has been reported to correlate with the DCMM activity [32–34]. A following study combining Raman spectroscopy, density functional theory (DFT) and normal coordinate analysis calculations identified the origin of the absorption band at 22700 cm^{-1} as a bent mono-(μ-oxo)dicupric site (illustrated in Figure 2.2a), which therefore has been suggested to be the active site for DCMM [58]. Although the assignment is strong, the initial correlation is not free from debate and thus further studies need to be carried out to test the hypothesis.

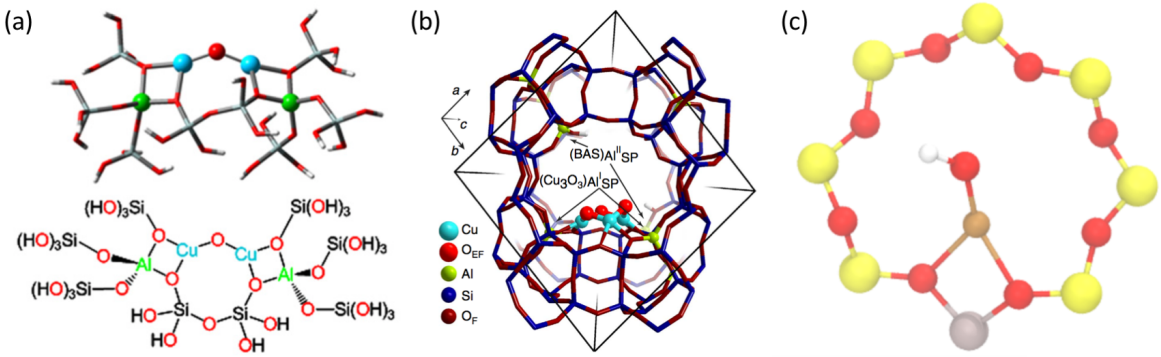

Figure 2.2: Illustration of proposed active sites for DCMM. (a) Cu dimer in Cu-ZSM-5, adapted from [58]. (b) Cu trimer in Cu-MOR, adapted from [38]. (c) Cu monomer in Cu-exchanged small pore zeolites, adapted from [59].

Nevertheless, it is still a challenge to complete the catalytic cycle with an acceptable degree of methane conversion [48, 49].

Unlike Cu-ZSM-5, the identification of active site for Cu-MOR seems to be more difficult. Studies have shown different reactivity towards DCMM on Cu-MOR depending on the reaction temperature [33] and activation conditions (with or without water vapour) [37]. These results indicate the existence of more than one type of active site. The structures of the active sites, however, have not yet been identified. Combined studies of X-ray adsorption spectroscopy (XAS) and DFT have been carried out to investigate the nature of the dicopper and tricopper cores (shown in Figure 2.2b) in mordenite, which are the proposed possible active sites for DCMM [38, 60]. Moreover, DCMM reactivity on small copper clusters in mordenite was observed under an isothermal condition [50], suggesting a possibly higher flexibility in catalyst design than first suggested based on early studies on Cu-ZSM-5 catalysts.

Small-pore zeolites and zeotypes have also been tested for DCMM. Materials such as Cu-chabazite and Cu-SAPO (silico-alumino-phosphate) have shown higher production of methanol compared to Cu-ZSM-5 [39]. However, further studies are needed to understand the reason behind the reported higher activity. The dominant Cu monomer sites in small pore zeolites suggests the possibility of yet another active site: $[Cu\text{-}OH]^+$, as shown in Figure 2.2c [59].

Other metal-containing zeolites

Fe-zeolites, as the earliest model for MMOs [40, 41], have received much attention. The active sites for methane dissociation was recognized as a surface oxygen species called α-oxygen. Early studies have explored topics such as modelling of the active sites [42, 61], using molecular oxygen for catalyst activation [62] and exploring the mechanisms [43, 44, 63–65]. However, no consensus prevail regarding the structure of the α-sites. It is still unclear whether it is a mononuclear or binuclear site [42, 44, 61–63].

Studies on DCMM over Co-ZSM-5 has been started less than ten years ago and have not drawn much attention yet. Mainly molecular oxygen was used as oxidant during DCMM. Selectivity towards methanol was reported to be related to larger cobalt oxide domains; while selectivity towards formaldehyde, as the other main product, is associated with Co ions at the ion-exchange positions [45, 66]. Understanding of topics

such as reaction mechanisms [46] and the influence of zeolites pore structures [47] are progressing slowly.

2.2.2 Challenges in gas phase DCMM over metal-exchanged zeolites

The challenges in DCMM can be summarized in two aspects: activation of methane and controlled oxidation to methanol. Activation of methane is difficult due to its strong and localized C-H bond (413 kJ/mol) [67]. Therefore, high energy input or a strong oxidation catalyst is required for initiating this reaction. However, this requirement is rather contradictory to the needs for a controlled partial oxidation to methanol, as the reaction intermediate can easily undergo further oxidation. While high energy input would not be desirable, the mission lies on finding a suitable catalyst for DCMM.

The ion-exchanged zeolite catalysts designed today could resolve both challenges to some extent. These materials, however, have their own limits, which in turn bring other challenges. The approach for gas phase DCMM nowadays mainly relies on the activation-oxidation-extraction sequence, which, strictly speaking, is a stoichiometric reaction rather than a catalytic cycle. Although catalytic production of methanol is possible in some specific cases, the methanol production rate is extremely low (below 55 μmol g^{-1} h^{-1}) [49, 68]. Therefore, it is essential to identify and understand these challenges thoroughly for the purpose of designing a realistic catalyst for DCMM.

Catalyst activation

In order to obtain and restore the active sites in functionalized zeolites that could tackle both methane activation and controlled oxidation to methanol, activation of the materials with oxidants (O_2, N_2O or NO) under elevated temperature is often needed. This results in non-isothermal reaction sequence. It is, however, possible to observe low temperature (150 - 200 °C) isothermal reaction using a specific oxidant (NO) [48], under elevated methane partial pressure [50] or with compromised reaction rate [49]. Generally, to obtain the active sites for DCMM, the catalyst needs to be treated under fairly specific conditions. The characteristics of the active sites and the changes they may go through during the reaction are yet to be explored.

Active sites

Once the active sites are formed, the functionalized zeolites are able to convert methane to methanol stoichiometrically with fairly low methanol production [32–35, 48, 49]. Even though continuous production of methanol is possible in specific cases, the reaction rate is extremely low [49]. Both concentration of the active sites and the regeneration of them are limiting factors to DCMM. For Cu-ZSM-5, only approximately 5 % of the Cu in the material contributes to methanol production [32, 33]. While the turn over number (TON) for Fe-ZSM-5 is only around 2 to 6.9, indicating blocking of the active sites [44, 65]. Since the structure of the active sites are still unclear, it is challenging to design a catalyst with higher concentration of active sites. Meanwhile, active sites regeneration is closely related to product removal and catalyst activation.

Methanol extraction

As product related species are formed at the active sites, chemical extraction is necessary for methanol removal. The species formed after oxidation step is commonly believed to be methoxy groups [46, 64, 65]. Therefore, addition of proton to the methoxy groups as well as replacement on the methoxy bonded catalytic sites are essential for methanol production. In such case, the stability of the adsorbed methoxy groups become a barrier for methanol forming. Consequently covering of active sites with extractor species terminates the reaction.

CHAPTER 3
METHODS

3.1 Catalyst preparation

3.1.1 Incipient wetness impregnation

For incipient wetness impregnation, a dry powder (often the support material) is mixed with a solution containing the precursor of the active phase. The solution is added drop-wise. The volume of the solution needs to be equivalent to the pore volume of the powder to be mixed with, in order to achieve a homogeneous impregnation of the support and thus even distribution and dispersion of the active phase. Finally, the powder is dried and calcined. A desired metal loading can be managed using this method. The alumina supported Pd-Pt and silica supported Cu samples discussed in this work were prepared using incipient wetness impregnation. Details of the metal loading and calcination conditions are described in chapter 4.

3.1.2 Aqua ion-exchange

For introducing Cu to the zeolite as charge-compensating cations, aqua ion-exchange (AIE) is often used. A parent zeolite is mixed with Cu salt solution and stirred for certain time to facilitate ion-exchange. An elevated temperature can be applied during ion-exchange. The pH value of the solution needs to be kept at certain value. Finally, the liquid is filtered and dried. All Cu-ZSM-5 samples were prepared using AIE as described in paper III.

3.2 *Ex situ* characterization

3.2.1 X-ray diffraction

X-ray diffraction (XRD) is commonly used to determine crystal structure and particle size. In this technique, X-ray radiation incident on the spinning sample surface from a range of angles. Reflection of the elastically scattered X-rays are then detected by a rotating detector positioned on the other side of the sample. Reflection occurs only when the scattered X-rays interferes constructively, which is described by the Bragg's Law [69]:

$$n\ \lambda = 2\ d\ sin\theta \tag{3.1}$$

where n is any integer, λ is the wavelength of the incident X-rays, d is the spacing between the crystal planes, and θ is angle between the incident X-rays and the crystal planes. In powder samples, different crystal planes are randomly oriented. By scanning a range of incident angles, reflection occurs from planes that are oriented at the correct angle and fulfill the Bragg's Law. From the powder diffraction patterns obtained, the d spacing of each reflection can be calculated. Furthermore, an estimation of the crystal size can be obtained using the Scherrer equation [70].

In this work, XRD is used for confirming the crystal structure of the Cu-ZSM-5 samples after AIE (paper III), as well as determine the crystal structure and particle size of the Pd-Pt alloy in alumina supported Pd-Pt samples (paper I).

3.2.2 Nitrogen physisorption

Nitrogen physisorption is often used for determining surface area and pore volume of porous materials. The measurement is performed at a constant temperature where the volume of nitrogen adsorbed or desorbed are measured at a range of pressures to form adsorption and desorption isotherms. The Brunauer–Emmett–Teller (BET) theory [71] is commonly used for analyzing specific surface area. The theory is based on the assumption that a monolayer of the adsorbate is formed on the measured material (adsorbent), followed by the successive layers adsorbed with the adsorption energy equals to the energy of liquefaction. It has to be noted that BET analysis is not strictly applicable for microporous materials, such as zeolites, where a pore filling process accompanies monolayer formation at low pressure, which violates the monolayer formation

assumption. The values of BET surface area, however, can still be used for empirical comparisons for the same type of microporous material.

3.3 *In situ* and *operando* catalyst characterization

3.3.1 Fourier transformed infrared spectroscopy

Fourier transformed infrared (FTIR) spectroscopy is commonly used for identifying functional groups or surface species. This technique is based on the interaction between molecules and infrared (IR) radiation. Transition between vibrational levels of certain chemical bonds may occur upon absorption of IR photons with equivalent energy which can be represented by IR frequency or wavenumber. The transition energy of the vibrational levels depends on the mass of the atoms at each end of the chemical bond as well as the bond strength which can be affected by a range of factors, such as adjacent bonds or structures, adsorption sites or modes, and temperature. This means that the IR absorption frequency is unique for the chemical bonds or functional groups and is sensitive to changes around them. Therefore, IR spectroscopy provides the possibility of identifying different chemical bonds simultaneously as well as observing changes of the targeted species.

In FTIR spectroscopy, a broadband light beam shines into a Michelson interferometer, where the beam is split and directed to a fixed mirror and a moving mirror, as shown in Figure 3.1. The beams are then reflected by the mirrors and recombined with certain frequencies according to the light interferences caused by the moving mirror.

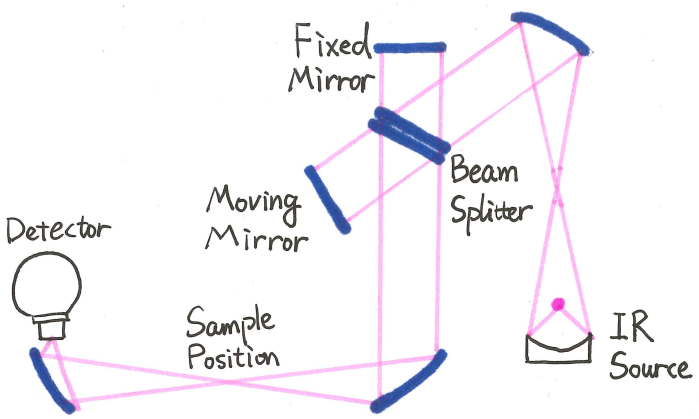

Figure 3.1: Sketch of an FTIR spectrometer setup

The recombined beam is directed through the sample to the detector, and raw data is summed as an interferogram. Afterwards, the interferogram (light absorption for each mirror position) is Fourier transformed into a desired spectrum (light absorption for each wavenumber).

In this work, FTIR is used for gas phase species identification during the flow reactor measurements, as well as surface species identification. More specifically, for surface species measurements, powder samples are measured under diffuse reflectance mode where the IR beam is reflected on the sample surface carrying surface species information. The technique is called diffuse reflectance infrared Fourier transform spectroscopy (DRIFTS).

3.3.2 X-ray absorption spectroscopy

X-ray absorption spectroscopy (XAS) is a widely used technique for determining the local structure of selected elements in matter. Due to its unique sensitivity of local structure and low requirement for sample environment, it has been well established as an *in situ/operando* characterization method for studying catalysts under realistic reaction conditions. XAS measurements are usually performed at a synchrotron radiation source for obtaining intensive and tunable X-ray. Figure 3.2 shows a type of XAS setup, where incident X-rays radiate on the sample with a certain range of monochromatic photon energies. When the incident photon energy is higher than the binding energy of a core electron, the photon is annihilated, transmitting its energy to a core electron cre-

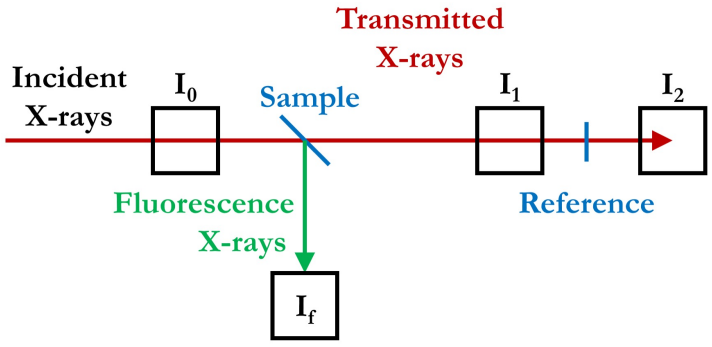

Figure 3.2: Example of an XAS measuring setup. I_0 - incident X-rays intensity; I_f - fluorescence X-rays intensity; I_1 - transmitted X-rays intensity after sample; I_2 - transmitted X-rays intensity after reference. The X-ray intensity is typically measured with ion chamber/CCD detectors.

ating a photoelectron and a core hole. The core hole is then filled by an electron from higher energy state releasing fluorescence X-rays. The relation between the absorption coefficient $\mu(E)$ and the measured X-ray intensity is:

$$\mu(E) \propto ln\frac{I_0}{I_1} \qquad \text{or} \qquad \mu(E) \propto \frac{I_f}{I_0} \tag{3.2}$$

XAS spectra are commonly measured at an absorption edge where the core electrons are excited from their bond states to the continuum, resulting in a sharp increase in absorption as shown in Figure 3.3 left panel. The region close to the absorption edge is called X-ray absorption near edge structure (XANES), where the spectrum shape reflects the excitation of core electron to its final states. In certain XANES spectra, the absorption edge appears to be a sharp intensive peak referred as "white line". Typically, XANES spectra are analyzed by comparing the measured spectrum with spectra of known structures, as so called "fingerprinting". The X-ray absorption spectrum region that is higher in energy than the absorption edge is called extended X-ray absorption fine structure (EXAFS), where the spectrum shape reflects the surrounding structure of the absorbing atoms. EXAFS can be used for obtaining information of different coordination shells after certain data processing. As shown in Figure 3.3 right panel, the peaks correspond to the different coordination shells in the Cu face centred cubic crystal structure.

In this work, XAS is used for studying the oxidation and reduction behaviour of alumina supported Pd-Pt alloy under methane oxidation conditions. More specifically,

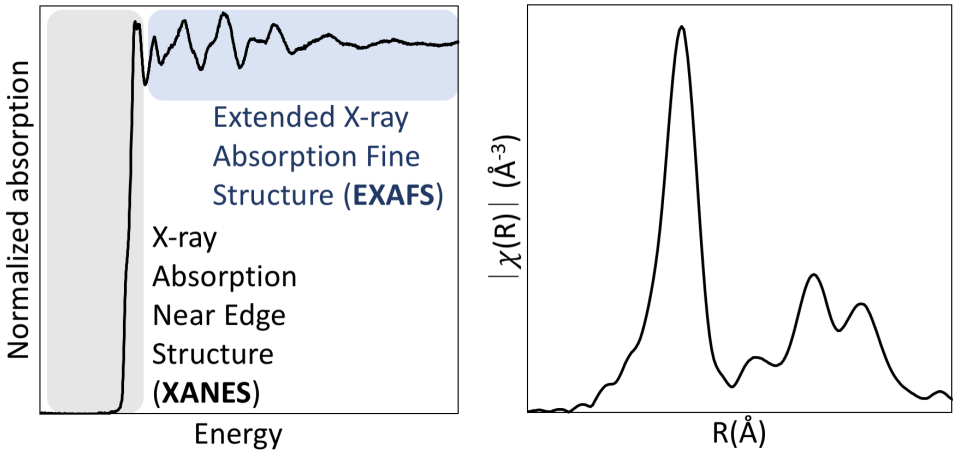

Figure 3.3: Left panel: normalized X-ray absorption spectrum of Cu foil. Right panel: Fourier transformed EXAFS spectra from Cu foil.

the chemical state of Pd and Pt is followed by XANES, while the local structure around Pt is investigated using Fourier transformed EXAFS spectra.

3.4 Catalyst evaluation with chemical flow reactor

A chemical flow reactor system is used for evaluating Cu-ZSM-5 as DCMM catalyst as well as following the desorbed gas phase species during temperature programmed desorption. The flow reactor consists of a horizontally mounted quartz tube surrounded by a heating coil. It is equipped with gas mixing system that consists of several mass flow controllers (Bronkhorst Hi-tech) and downstream gas phase analyzers. The gas mixing system and heating are controlled and monitored by use of Labview (National Instruments) program. The monolith sample is positioned close to gas outlet with two uncoated monoliths before and after for minimizing temperature gradients. By use of thermocouples, the reactor and catalyst temperature is measured inside the upstream uncoated monolith and the sample monolith, respectively. A CEM-system (controlled evaporator mixer; Bronkhorst Hi-tech) is used for injection of liquid reactants such as methanol. A separate water reactor that produces ultra-pure water vapor from catalytic reaction between H_2 and O_2 is installed to the feed gas system in the flow reactor as to eliminate possible risks of contamination during product extraction.

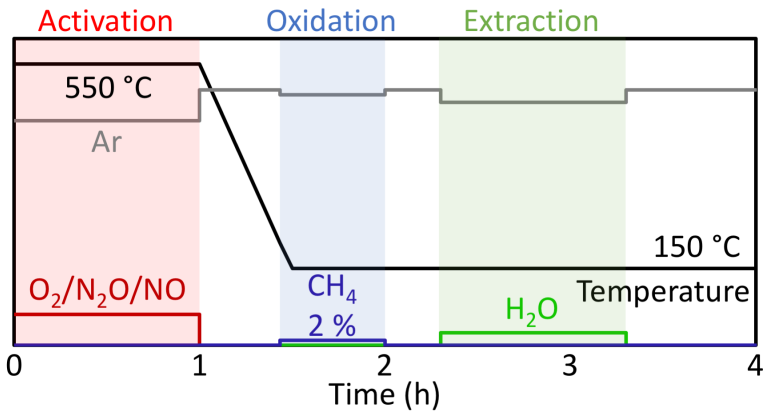

Figure 3.4: Sequential reaction conditions for DCMM in chemical flow reactor system.

3.4.1 Activity-selectivity tests

The activity test for DCMM is carried out through the activation-reaction-extraction sequential approach as shown in Figure 3.4. The samples are activated at 550 °C with oxidants (20% O_2, 300 ppm N_2O or 0.1% NO) for one hour before oxidation of 2% CH_4 at 150 °C. The products are then extracted with 4-8% of water vapor.

3.4.2 Temperature programmed desorption

Temperature programmed desorption (TPD) can be used to probe certain surface sites as well as to follow interaction between the adsorbates and the surface. The principle of TPD is described in Figure 3.5. Before measurement, a clean surface is obtained by calcination (Figure 3.5a), followed by adsorption of certain probing molecules at lower temperature (Figure 3.5b). After flushing in inert gas without the probe molecule, a linear heating rate is then applied and the desorbed gas phase species are recorded, an example shown in Figure 3.5c. This specific example illustrates the TPD profile of a simplified surface with two types of adsorption sites, weak adsorption site A and strong adsorption site B. With temperature increase, adsorbates bond with site A starts to desorb, followed by desorption from sites B at higher temperature. Two peaks are

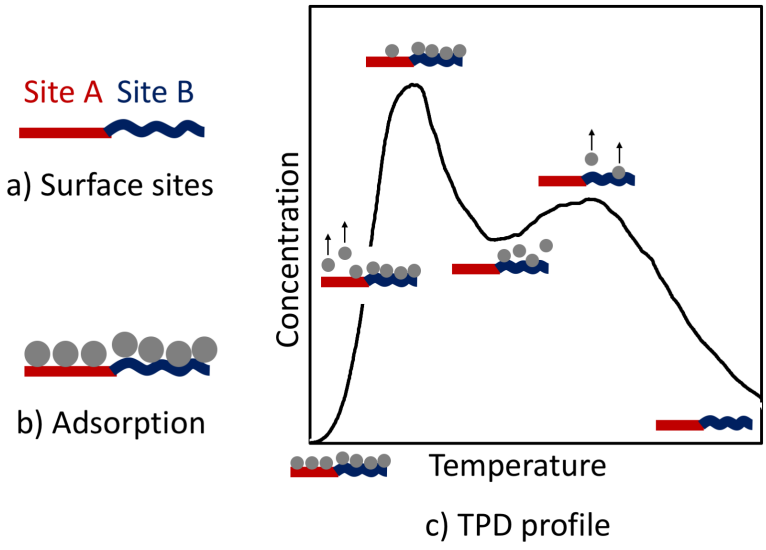

Figure 3.5: Schematic sketch of TPD: a) a simplified clean surface with two types of adsorption sites A and B; b) surface after adsorption; c) TPD profile with illustration of molecule desorption on the surface.

therefore formed in the TPD profile relating to these two sites. Generally, different desorption temperature indicates different types of adsorption sites. The binding energy of the adsorbates and certain sites can be calculated according to the desorption temperature. Additionally, intensity of the desorbed species on the vertical axis at certain temperatures indicates the amount of the species adsorbed. Therefore the integrated intensity of desorbed species in a certain temperature interval is proportional to the amount of certain adsorption sites.

As the activation of methane over Cu-exchanged zeolites being a great challenge, it is extremely difficult to obtain surface information during activation and thereby further knowledge on the kinetics. Furthermore, extraction of methanol remains a "black box" and may be a key to avoid the activation-oxidation-extraction sequence. Therefore, in this study we explored the interaction between methanol and Cu-ZSM-5 using methanol-TPD. Flow reactor experiments and DRIFTS are used for probing desorbed gas phase species and surface species, respectively, during desorption. For this method, samples are pretreated in O_2 at 550 °C for 1 h before methanol adsorption at lower temperature. For flow reactor experiments, the samples are exposed to methanol at about 76 °C until saturation. The desorbed gas phase species are then recorded using FTIR. For the DRIFTS measurements, the samples are exposed to methanol at 30 °C followed by stepwise methanol desorption and IR measurements at certain temperatures as described in Paper III.

CHAPTER 4

RESULTS AND DISCUSSION

4.1 Complete methane oxidation over Pd-Pt/Al_2O_3

In this work model catalysts, *i.e.*, Pd-Pt nanoparticles supported on alumina that has been calcined at different conditions, were studied for complete methane oxidation. The main findings are presented in paper I and II. In paper I, the formation/consumption of surface species and changes in chemical state and structural properties of the Pd-Pt nanoparticles are correlated to catalytic activity for methane oxidation under transient methane oxidation conditions. In paper II, a more detailed characterization of the chemical state and morphology of the nanoparticles and their responses to oxidative and reductive treatments were studied. The results published in paper I and II are summarized in this section.

From Figure 4.1 the changes in the presence of surface carbonyl species (top panels) and oxidation state of Pd (middle panels) in the Pd-Pt/Al_2O_3 model catalysts can be correlated to the measured effluent gas composition (bottom panels) under transient reaction conditions, *i.e.*, pulsed oxygen concentration. The Pd-Pt/Al_2O_3 catalysts were calcined in air at 500 and 800, and 800 °C in air with presence of 10% water, here denoted with F500 (left panles), F800 (middle panels) and L800 (right panels), respectively. As an indicator of the Pd oxidation state the white line intensity at Pd K-edge has been used as described in a previous study [72]. The observations during transient methane oxidation over the samples can be summarized as follows: i) the F800 sample has the highest activity under lean conditions, followed by the L800 and F500 samples;

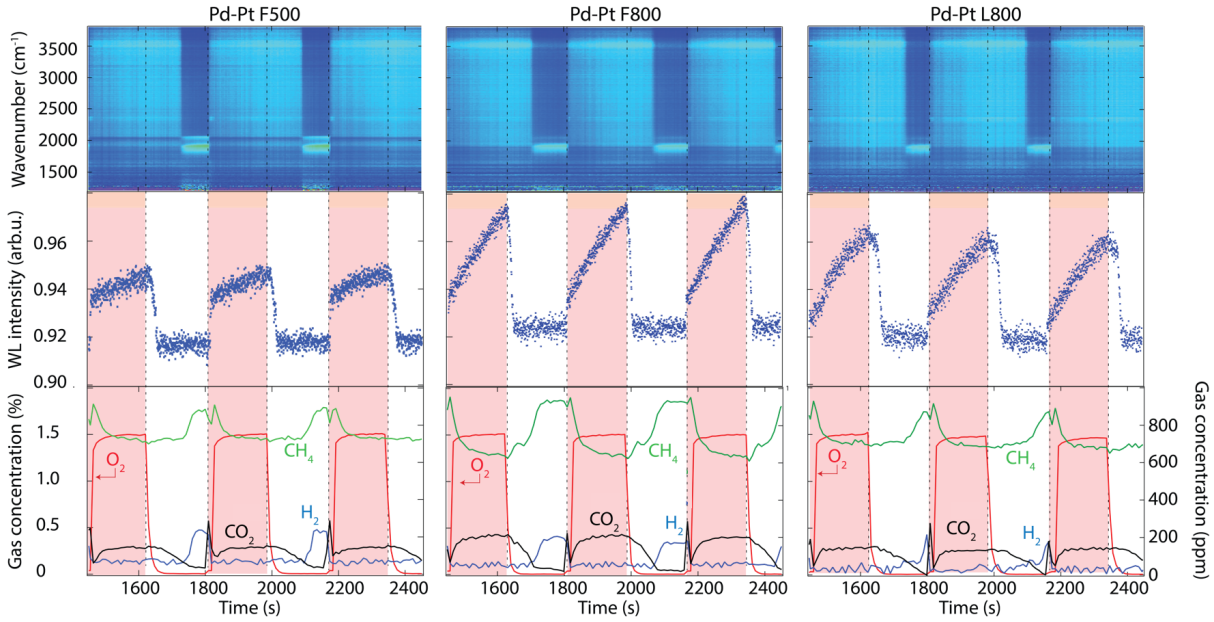

Figure 4.1: Transient methane oxidation over Pd-Pt/Al_2O_3 catalysts pretreated in air under 500 °C (left panels, Pd-Pt F500), 800 °C (middle panels, Pd-Pt F800), and 800 °C with 10% water presence (right panels, Pd-Pt L800). Top panels: color coded (blue corresponds to low intensity, red to high intensity) IR spectra. Middle panels: evolution of white line intensity at Pd absorption edge. Bottom panels: concentration of main gas phase species measured by mass spectrometry.

ii) the white line intensities of F800 and L800 increases gradually and continuously upon introducing O_2, which is different from F500; iii) the white line intensities drop sharply upon switching to rich conditions, indicating a reduction of PdO to Pd, which results in decreased activity; iv) PdO reduction also leads to carbonyl formation on the noble metals resulting in blocking of noble metal sites, and therefore complete lose of activity; v) carbonyl formation, PdO reduction and activity decrease upon switching to rich condition occurs the fastest for the F800 sample followed by the F500 and L800 samples.

It has been observed that the carbonyl spectra under rich condition for F500 exhibit two distinct absorption bands, while for F800 and L800 one band is more prominent, as shown in Figure 4.1 upper panels. Therefore, additional CO adsorption was performed for obtaining detailed surface information. Evolution of IR spectra for the F500, L800 and L800 samples upon CO adsorption for 10 min are shown in Figure 4.2. The band at 2051 cm^{-1} is assigned to linear CO adsorbed on mostly Pt [73], while the band at

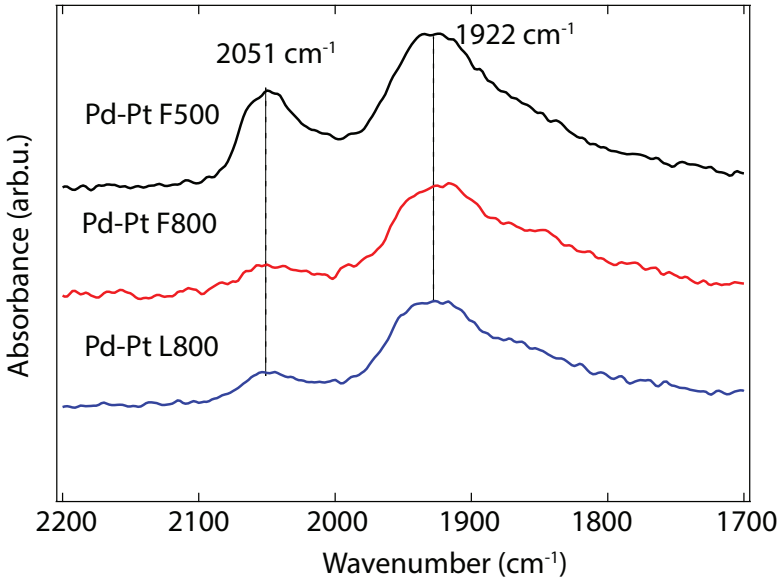

Figure 4.2: IR spectra for the F500 (black), F800 (red) and L800 (blue) samples exposed to 0.05% CO for 10 min after methane oxidation at 360 °C.

1922 cm^{-1} can be associated with bridged CO adsorbed on Pd [74, 75]. Both bands are prominent for the F500 sample, indicating availability of both Pd and Pt sites on the metal particle surface. While only the band of CO on Pd sites is pronounced for the F800 and L800 sample, suggesting the exposure of mainly Pd on the metal particle surface. These speculations are supported by the TEM and LEIS results shown in Paper II.

Characterization of the Pd-Pt/Al_2O_3 catalysts (paper II) suggest Pd-Pt alloy formation in the samples with higher calcination temperature (F800 and L800), while monometallic Pd and Pt particles are present in the sample calcined at lower temperature (F500). Moreover, an enrichment of Pt at the surface of the alloyed samples is observed under reducing conditions, while PdO phase dominates the particle surface under oxidizing conditions. Under rich methane oxidation conditions, both Pd and Pt remain reduced. Partial oxidation of methane dominates forming carbonyl on the catalyst surface. While under lean methane oxidation, Pd is oxidized to PdO and Pt tends to form metallic Pt in the alloy samples, which agrees with the results from a previous study [25]. Reversible changes of alloyed Pd-Pt nanoparticles are observed under transient methane oxidation conditions.

4.2 DCMM over Cu-zeolites

4.2.1 *Ex situ* characterization and activity tests

Figure 4.3a shows the XRD patterns of the Cu/SiO_2, Cu-SSZ-13 and Cu-ZSM-5 samples, and the parent H-ZSM-5. Characteristic reflections of crystalline CuO are present in the XRD patterns of Cu/SiO_2, indicating the existence of CuO particles in the Cu/SiO_2 sample. The XRD patterns of Cu-SSZ-13 and Cu-ZSM-5, however, exhibit the characteristic peaks of the ZSM-5 and SSZ-13 crystal structure respectively [76]. No reflections of crystalline Cu species are visible in these patterns suggesting high dispersion of the Cu species in Cu-SSZ-13 and Cu-ZSM-5 samples. The XANES spectra for the Cu-SSZ-13 and Cu-ZSM-5 samples overlap with each other, as shown in Figure 4.3b. Both spectra present a sharp absorption at about 8995-8998 eV, which is due to the 1s to 4p electronic transition of Cu(II) species [77]. No obvious pre-edge peak for Cu(I) (well defined peak at 8982-8984 eV [77, 78]) can be observed, indicating the oxidation state of Cu species is dominantly Cu(II) in both samples. The featureless pre-edge, however, eliminates the existence of CuO like structure (weak absorption at about 8976-8979 eV and shoulder at about 8985-8988 eV [78]), indicating that the Cu-SSZ-13 and the Cu-ZSM-5 samples do not contain detectable amount of large Cu domains. The XAS results agree with the results from the XRD analysis for Cu-SSZ-13 and Cu-ZSM-5, suggesting that isolated Cu ions are dominant in both samples.

Activity test for DCMM was carried out in the chemical flow reactor system through the activation-reaction-extraction sequence described in Chapter 3.4. Methanol as the main product, is present in Figure 4.3c, where the methanol production is acquired by applying peak area integration to the original methanol FTIR signal (shown in appendix Figure A1) during water extraction, followed by subtraction of the amount of methanol produced over H-ZSM-5 with corresponding oxidants. Materials containing different Cu species, *i.e.* Cu ions or CuO particles, have been tested for DCMM with various oxidants. All samples show low amounts of methanol during water extraction. The methanol production over the Cu-ZSM-5 (regardless of oxidant) and Cu-SSZ-13 (oxidized by O_2 or N_2O) samples, however, is clearly higher than that over Cu/SiO_2 or H-ZSM-5. The same results are clearly noticeable from the FTIR signal (appendix Figure A1). The Cu-ZSM-5 and Cu-SSZ-13 samples consist mainly of isolated Cu ions, ZSM-5 framework sites as

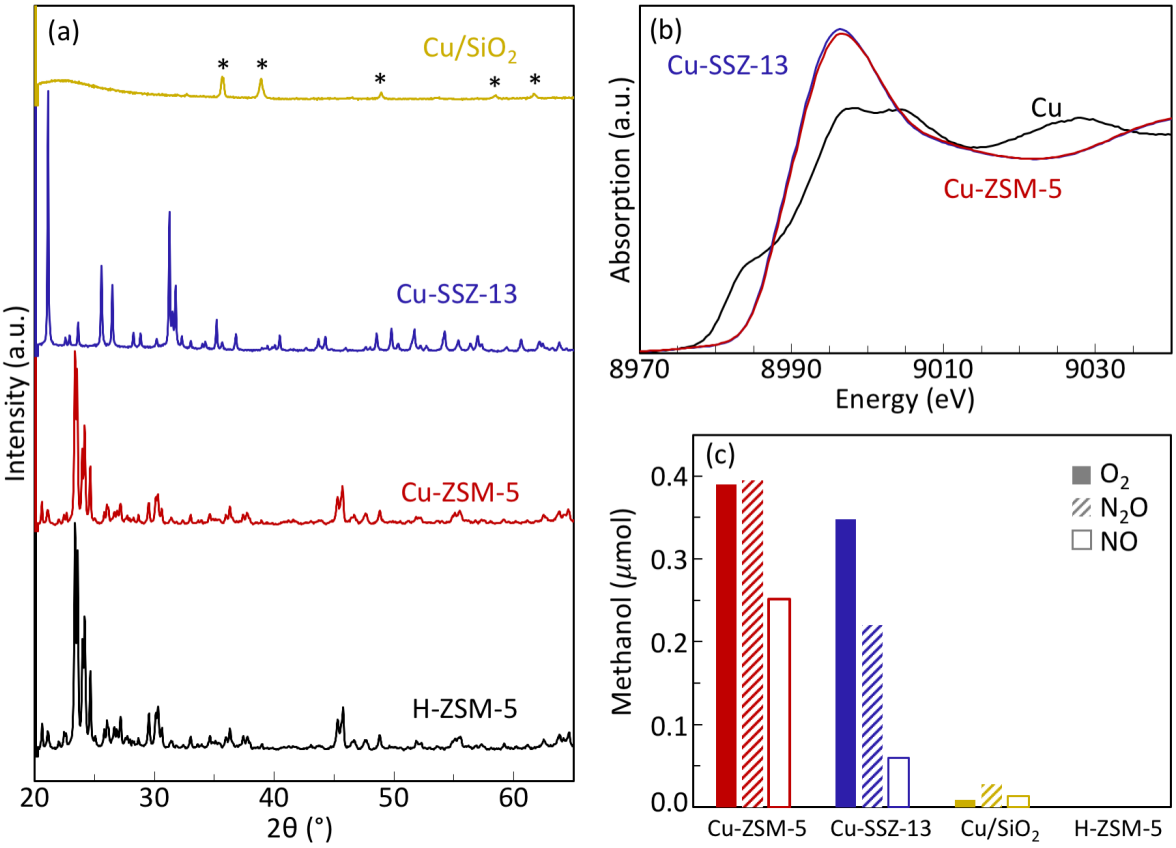

Figure 4.3: (a) XRD patterns for the Cu/SiO_2, Cu-SSZ-13 and Cu-ZSM-5 samples and the parent H-ZSM-5; the characteristic reflections of the CuO crystalline structure are denoted with asterisks. (b) XANES spectra of the Cu-SSZ-13 and Cu-ZSM-5 samples; spectrum of Cu foil is included as reference. (c) Methanol production over Cu-ZSM-5, Cu-SSZ-13, Cu/SiO_2 and H-ZSM-5 using O_2, N_2O or NO as oxidants

well as zeolitic defects, while the Cu/SiO_2 sample dominantly contains of Cu particle sties and silica sites. Therefore, the higher methanol production from Cu-ZSM-5 and Cu-SSZ-13 compared with Cu/SiO_2 and H-ZSM-5 can be attributed to the isolated Cu ions, which is in consistency with previous studies [33,58,59,79–82]. It should be mentioned that due to the low methanol concentrations, one should be careful with quantitative analysis and instead interpret the experimental activity results in a qualitative manner.

4.2.2 Methanol desorption

DCMM over heterogeneous catalysis, as a great challenge in modern chemistry, can not be simply studied only using conventional trial and error based methods. For a thorough solution to the activation-oxidation-extraction approach, it is necessary to obtain deeper understandings on each step of the reaction cycle. Therefore, in this work we explored the interaction between Cu containing materials and methanol using methanol-TPD.

TPD profiles

As the main species desorbed during methanol-TPD at lower temperatures, the desorption spectra of methanol and DME from Cu-ZSM-5 samples with different ion-exchange time are presented in Figure 4.4. The results from the parent H-ZSM-5 sample and Cu/SiO_2 are included as reference. The desorption spectra of CO and CO_2 are shown in the appendix Figure A2.

The desorption profile of methanol for all Cu-ZSM-5 samples (Figure 4.4 left panel) exhibits desorption peaks with higher intensity and broader width at higher temperatures compared with H-ZSM-5 and Cu/SiO_2. The higher intensity of the methanol desorption peaks for the Cu-ZSM-5 samples compared with their parent zeolite H-ZSM-5 suggests that the Cu species in ZSM-5 are responsible for the additional methanol adsorption, while the methanol desorption at higher temperature for the Cu-ZSM-5 samples indicates that some of the Cu species in ZSM-5 bind stronger with methanol compared to other sites in the parent H-ZSM-5. Similar conclusions can be drawn comparing the methanol desorption spectra of the Cu-ZSM-5 samples and Cu/SiO_2: the isolated Cu ions in ZSM-5 interact stronger with methanol than CuO particles in SiO_2.

During methanol-TPD, DME is formed due to methanol dehydration on the acidic sites of the samples [83, 84]. Compare to H-ZSM-5 and Cu/SiO_2, the DME desorption profiles for the Cu-ZSM-5 samples exhibit the main desorption peak of DME at higher

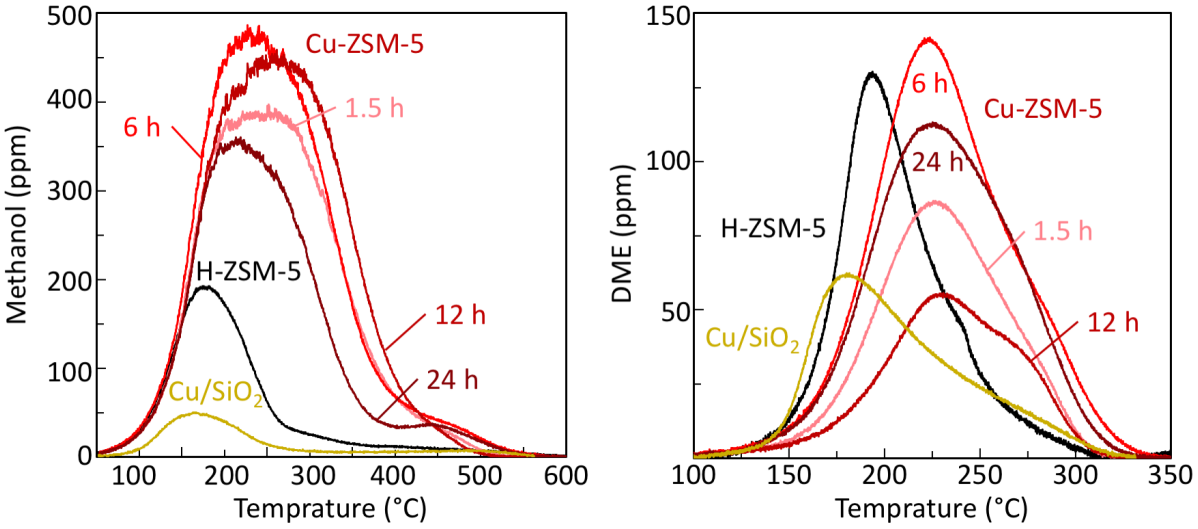

Figure 4.4: Desorbed gas phase species during methanol-TPD from Cu-ZSM-5 with different ion-exchange time (marked as x h in red), H-ZSM-5 (black) and Cu/SiO_2 (yellow). Left panel: methanol; right panel: DME.

temperatures. On the one hand, the lower amount of DME desorption at lower temperatures (below 200 °C) for the Cu-ZSM-5 samples compared to the H-ZSM-5 sample may be due to covering of Cu ions on Brønsted acid sites and framework defects in the Cu-ZSM-5 samples during the ion-exchange. On the other hand, dehydration of the strongly bond methanol forming DME occurs at higher temperatures for the Cu-ZSM-5 samples, suggesting that methanol and its derivative species interact more strongly with some isolated Cu species in Cu-ZSM-5. Moreover, the comparison between the DME desorption profile for Cu/SiO_2 and the Cu-ZSM-5 samples reinforces that isolated Cu species take responsibility of the strong interaction with methanol and its derivative species rather than CuO particles.

Although the desorption of methanol and DME from the Cu-ZSM-5 samples with different ion-exchange time exhibits similarity in the shape of the desorption profiles, there are still considerable differences in intensities of the desorption spectra. These varieties may due to different composition of Cu species in the samples. However, no obvious trend can be observed along ion-exchange time, indicating that more parameters are involved during the ion-exchange process. Unfortunately, identification of the Cu species in the Cu-ZSM-5 samples are not feasible due to lack of experimental references. Experiments on controllable Cu containing samples as well as theory studies of this system maybe necessary for seeking solutions.

Evolution of surface species

As methanol-TPD measurements in the flow reactor system reveal the interaction of methanol with Cu-ZSM-5 by analysing desorbed gas phase species, information of the sample surface remains unknown. Therefore, we explored the dynamic interaction of methane and its derivatives with our Cu containing samples and H-ZSM-5 during methanol desorption using *in situ* DRIFTS. Paper III includes characterization and the DRIFTS measurements for the Cu-ZSM-5 samples and its parent H-ZSM-5. In this section the results in Paper III are summarized.

Paper III contains assignments for all important surface species during methanol desorption. The main objectives of Paper III are to establish a steppingstone as reference for future studies on similar systems as well as to seek reasons for necessity of methanol extraction during DCMM. Figure 4.5 presents an example of one set of DRIFT spectra taken during methanol-TPD from Cu-ZSM-5.

The entire methanol desorption process from Cu-ZSM-5 and its parent H-ZSM-5 can be summarized as follows. Upon introduction of methanol, weak interactions between the zeolite framework and methanol are formed, resulting in methanol related

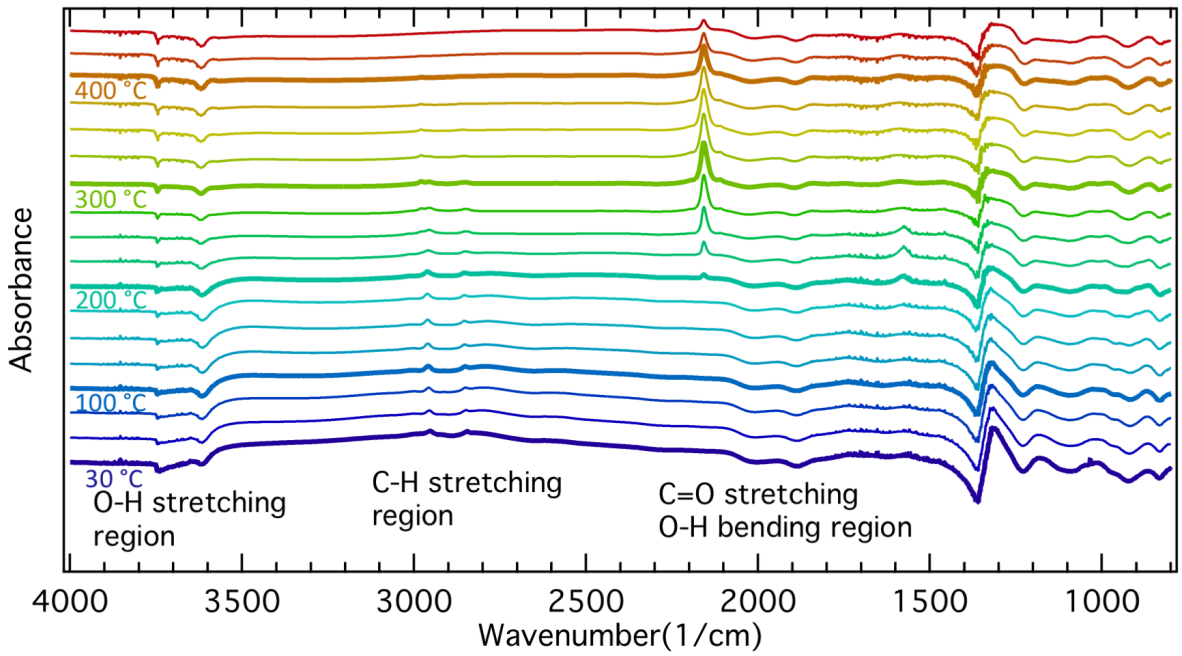

Figure 4.5: Series of selected DRIFT spectra collected during methanol-TPD from 30 to 450 °C in Ar from Cu-ZSM-5 with 24 hours ion-exchange time.

C-H stretching bands and perturbed zeolitic O-H vibrations in the DRIFT spectra of both the Cu-ZSM-5 and the H-ZSM-5 sample. Some negative peaks in the O-H stretching region are related to methanol adsorption on the defects in the zeolite framework structure and acidic sites in H-ZSM-5. These peaks are absent in the spectra for the Cu-ZSM-5 sample, indicating replacement of the protons in hydroxyl groups at zeolitic defects and the Brønsted acid sites with Cu ions due to the ion-exchange. Additionally, dehydration of methanol takes place directly after methanol adsorption forming water on Cu-ZSM-5, generating the water deformation band. The absence of this band in the H-ZSM-5 sample spectra suggests that low-temperature dehydration of methanol takes place at the Cu sites. With increasing temperature, the liquid-like methanol desorbs and stronger interactions begin to form on both samples. For the H-ZSM-5 sample spectra, methoxy groups become observable on extra framework Al sites in H-ZSM-5 at 150 °C followed by DME formation over the Brønsted acid sites at 200 °C. Whereas for the Cu-ZSM-5 sample, due to the Cu ions on the ion-exchange sites, these bands are less evident. Formation of formate and CO, however, is evident for Cu-ZSM-5 only, suggesting further oxidation of methanol and methoxy groups on the Cu sites. At temperature above 300 °C, methoxy groups bound at with Brønsted acid sites and silanol groups become prominent for both samples. These bands remain with compromised intensity at 450 °C indicating that methoxy groups bind strongly on the ZSM-5 framework.

The conclusions for Paper III can be summarized as follows: i) the Brønsted acid sites and defects in the framework structure of the zeolite, *i.e.* extra framework Al and silanol groups, constitute ion-exchange sites for Cu ions; ii) the Cu species in Cu-ZSM-5 are responsible for interaction with methanol that is additional to the methanol adsorbed on the ZSM-5 framework sites, in consistency with the methanol desorption profile shown in Figure 4.4; iii) the Cu species in Cu-ZSM-5 are responsible for further oxidation of methanol and methoxy groups to formate and CO, resulting in higher CO and CO_2 desorption at higher temperatures (Appendix Figure A2); iv) strong interactions are observed between methoxy groups and some zeolitic framework sites, *i.e.* the Brønsted acid sites and silanol groups, suggesting the necessity of the proton extraction step during direct partial oxidation of methane to methanol over Cu-ZSM-5.

CHAPTER 5
CONCLUSIONS AND OUTLOOK

5.1 Conclusions

This thesis includes studies on complete methane oxidation over alumina supported alloy Pd-Pt nanoparticles and partial methane oxidation over Cu-functionalized zeolites.

For complete methane oxidation, the activity of Pd-Pt/Al_2O_3 samples with different calcination conditions was investigated under transient methane oxidation conditions. Reversible changes in nanoparticle structure and chemical state were observed under switching between lean and rich conditions. The conclusions are as follows: i) high calcination temperature (800 °C) results in Pd-Pt alloy formation, while low calcination temperature (500 °C) leads to isolated monometallic nanoparticles; ii) higher activity for methane oxidation was observed over the alloy Pd-Pt samples compared with the non-alloy sample under lean conditions; iii) the activity for methane oxidation follows the the formation of PdO, indicating PdO being the most active phase in Pd-Pt/Al_2O_3; iv) Pt enrichment occurs under reducing conditions while PdO dominates at the surface of alloyed nanoparticles under oxidizing conditions; v) both Pd and Pt are reduced under rich methane oxidation condition while oxidized Pd and reduced Pt are present under lean methane oxidation condition; vi) all changes in structure and chemical state of the Pd-Pt/Al_2O_3 samples during transient conditions are reversible.

For partial methane oxidation to methanol, Cu-exchanged zeolites were tested for DCMM activity. Moreover, dynamic interactions between methanol and Cu-exchanged zeolites were investigated for further understanding of the reaction cycle. The conclu-

sions of this part can be summarized as follows: i) isolated Cu ions on ion-exchange sites in the zeolite framework structure are responsible for the DCMM activity, while Cu particles are not active; ii) isolated Cu ions on ion-exchange sites in the zeolite framework structure take most of the responsibilities for the stronger interactions with methanol and its derivatives during methanol-TPD; iii) the Brønsted acid sites and defects in the framework structure of the zeolite provide possible ion-exchange sites for Cu ions; iv) the Cu species in Cu-ZSM-5 are responsible for further oxidation of methanol and methoxy groups to formate and CO, resulting in higher CO and CO_2 desorption at higher temperature; v) strong interactions are formed between methoxy groups and some zeolitic framework sites, suggesting the necessity of the proton extraction step during direct partial oxidation of methane to methanol over Cu-ZSM-5.

5.2 Outlook

As Pd based catalysts are overwhelmingly active for complete methane oxidation, more efforts can be put on engineering Pd containing catalysts that expose higher amount of active sites and are more resistant to sintering and poisoning. Using porous supports such as zeolites or mesoporous silica may serve some of these purposes.

For partial oxidation of methane to methanol, methane dissociation and selectivity towards methanol favours contradictory properties of the catalytic material. Based on our current knowledge, both active sites and support materials play important roles in this reaction. Controlled manufacturing of zeolites with certain Al distributions may provide possible ion-exchange sites that leads to increased amount of active Cu centres. As zeolite structures stabilize the methoxy groups and prevent them from further oxidation, it is also difficult to obtain the final product methanol. Proton extraction is necessary according to our work, and the proton sources we are using now are water or other organic compounds with easily dissociated protons. This extraction process in turn brings in unwanted hydroxyl groups, blocking the Cu centres, and therefore terminates the reaction. To avoid blockage of active sites, it may be reasonable to find a proton source that does not introduce other unwanted species. Another strategy may be to introduce elements that are more active for methane activation such as Pd or Pt into the zeolite structures.

Acknowledgements

The research presented in this thesis was carried out at the Division of Applied Chemistry and the Competence Centre for Catalysis (KCK), Chalmers University of Technology, Göteborg, Sweden, during the period of August 2014 to March 2017.

This work is financially supported by the Swedish Research Council through the Röntgen-Ångström collaborations "Catalysis on the atomic scale" (No. 349-2011-6491) and "Time-resolved in situ methods for design of catalytic sites within sustainable chemistry" (No. 349-2013-567), and the Swedish Energy Agency through the FFI program “Fundamental studies on the influence of water on oxidation catalyst for biogas applications” (No. 40274-1).

The Competence Centre for Catalysis is hosted by Chalmers University of Technology and financially supported by the Swedish Energy Agency and the member companies: AB Volvo, ECAPS AB, Haldor Topsøe A/S, Volvo Car Corporation AB, Scania CV AB, and Wärtsilä Finland Oy.

Part of the research has been carried out at MAX IV Laboratory (Lund, Sweden) and the European Synchrotron Radiation Facility (ESRF) (Grenoble, France). I would like to thank beamline I811 (MAX IV Laboratory) and ID24 (ESRF) for providing the beamtime and the beamline staffs for their assistance.

Additionally I would like to thank:

My main supervisor Per-Anders Carlsson, for all the guidance, support and creative ideas. Working with you is always pleasurable and fun. I appreciate the feedback from all the things I sent to you: poster, manuscript, abstract, presentations... All feedback from you have been positive and constructive for my growth as a researcher. Thank you for your understanding and help through my way towards this licentiate.

My co-supervisors, Magnus Skoglundh and Anders Hellman, for many discussions and questions from different views. You influenced me as a scientist to always think outside of my "box".

Hanna Härelind, Ann Jokobsson and Frida Andersson, for all the help and many events you organized.

My theoretician Adam Arvidsson. I am often inspired by you both about the topic we are working on as well as in the way of thinking and communicating. I am looking forward to working with you for longer time.

My collaborators Johan Gustafson and Chu Zhang, for the discussions and suggestions at the symposia, as well as your kind guidance during the time at PETRA III and MAX IV Laboratory.

My fellow colleagues of KCK and TYK, current or past, for the fun we had together. I appreciate your company for all the conferences we joined, hikes we went, port wines and beers we drank, sports we participated, games we played, sauna we enjoyed, life we discussed and of course the "fika" we took. Special thanks go to (alphabetic order): Alexander Shishkin, Alina, Alvaro, Anand, Carl-Robert, Caroline, Colin, Emma Adams, Felix, Giulio, Gunnar, Ida Friberg, Johan Nilsson, Johanna Englund, Marika, Matthias, Mattias, Maxime, Mikael, Mikkel, Milene, Natalia, Peter, Ron, Saba, Sam, Simon Isaksson, Simone and Soheil.

People that inspired, encouraged and influenced me and my life in Gothenburg: Adriano, Anna-Karin J. Sjöberg, Daniel Larsson and Melanie.

Last but not the least, my parents, for your support and your encouragements.

Xueting Wang, Göteborg, March 2017

BIBLIOGRAPHY

[1] *International Association for Natural Gas Vehicles*, Retrieved 2017-04-18, **http://www.iangv.org/current-ngv-stats/**.

[2] *Gas South Compressed Natural Gas*, Retrieved 2017-04-18, **https://www.gas-south.com/business/compressed-natural-gas.aspx**.

[3] V. Ramaswamy, O. Boucher, J. Haigh, D. Hauglustaine, J. Haywood, G. Myhre, T. Nakajima, G. Shi, and S. Solomon, *Intergovernmental Panel on Climate Change*, 2001, **Ch. 6.12**, 385.

[4] C. Teetz, *CIMAC Central Secretariat*, 2014.

[5] R. A. B. Semin, *American Journal of Engineering and Applied Sciences*, 2008, **1**(4), 302–311.

[6] J. Chen, H. Arandiyan, X. Gao, and J. Li, *Catalysis Surveys from Asia*, 2015, **19**, 140–171.

[7] Z. Zakaria and S. Kamarudin, *Renewable and Sustainable Energy Reviews*, 2016, **65**, 250–261.

[8] M. J. da Silva, *Fuel Processing Technology*, 2016, **145**, 42–61.

[9] A. Satsuma, K. Osakia, M. Yanagiharaa, J. Ohyama, and K. Shimizu, *Catalysis Today*, 2015, **258**, 83–89.

[10] A. Hellman, A. Resta, N. M. Martin, J. Gustafson, A. Trinchero, P. A. Carlsson, O. Balmes, R. Felici, R. van Rijn, J. W. M. Frenken, J. N. Andersen, E. Lundgren, and H. Grönbeck, *The Journal of Physical Chemistry Letters*, 2012, **3**(6), 678–682.

[11] S. Colussi, F. Arosio, T. Montanari, G. Busca, G. Groppi, and A. Trovarelli, *Catalysis Today*, 2010, **155**, 59–65.

[12] D. Bounechada, S. Fouladvand, L. Kylhammar, T. Pingel, E. Olsson, M. Skoglundh, J. Gustafson, M. Di Michiel, M. A. Newton, and P. A. Carlsson, *Physical Chemistry Chemical Physics*, 2013, **15**(22), 8648–61.

[13] I. Y. Pakharukov, A. Y. Stakheev, I. E. Beck, Y. V. Zubavichus, V. Y. Murzin, V. N. Parmon, and V. I. Bukhtiyarov, *ACS Catalysis*, 2015, **5**, 2795–2804.

[14] E. Becker, P. Carlsson, H. Gronbeck, and M. Skoglundh, *Journal of Catalysis*, 2007, **252**(1), 11–17.

[15] P.-A. Carlsson, E. Fridell, and M. Skoglundh, *Catalysis Letters*, 2007, **115**(1-2), 1–7.

[16] P.-A. Carlsson, M. Nordström, and M. Skoglundh, *Topics in Catalysis*, 2009, **52**(13-20), 1962–1966.

[17] K. Persson, A. Ersson, S. Colussi, A. Trovarelli, and S. Järås, *Applied Catalysis B: Environmental*, 2006, **66**(175-185).

[18] G. Lapisardi, P. Gélin, A. Kaddouri, E. Garbowski, and S. D. Costa, *Topics in Catalysis*, 2007, **42-43**, 461–464.

[19] A. K. Khudorozhkov, A. V. Bukhtiyarov, E. Y. Gerasimov, I. P. Prosvirin, and V. I. Bukhtiyarov, *Russian Chemical Bulletin, International Edition*, 2015, **64**(12), 2802–2805.

[20] H. Yamamoto and H. Uchida, *Catalysis Today*, 1998, **45**, 147–151.

[21] R. Strobel, J.-D. Grunwaldt, A. Camenzind, S. E. Pratsinis, and A. Baiker, *Catalysis Letters*, 2005, **104**, 9–16.

[22] G. Lapisardi, L. Urfels, P. Gélin, M. Primet, A. Kaddouri, E. Garbowski, S. Toppi, and E. Tena, *Catalysis Today*, 2006, **117**, 564–568.

[23] G. Corro, C. Cano, and J. Fierro, *Journal of Molecular Catalysis A: Chemical*, 2010, **315**, 35–42.

[24] P. Castellazzi, G. Groppi, and P. Forzatti, *Applied Catalysis B: Environmental*, 2010, **95**, 303–311.

[25] N. M. Kinnunen, J. T. Hirvi, M. Suvanto, and T. A. Pakkanen, *Journal of Molecular Catalysis A: Chemical*, 2012, **356**, 20–28.

[26] Y. Ji, G. Mao, Y. Wang, and M. Bartlam, *Frontiers in Microbiology*, 2013, **4**, 58.

[27] C. Citek, J. B. Gary, E. C. Wasinger, and T. D. Stack, *Journal of American Chemical Society*, 2015, **137**(22), 6991–4.

[28] *Protein Data Bank in Europe*, 2014, **http://www.ebi.ac.uk/pdbe/entry/pdb/4pi2**.

[29] T. Splettstoesser, 2015, **https://commons.wikimedia.org/wiki/File%3AZeolite-ZSM-5-vdW.png**.

[30] C. Hammond, N. Dimitratos, J. A. Lopez-Sanchez, R. L. Jenkins, G. Whiting, S. A. Kondrat, M. H. ab Rahim, M. M. Forde, A. Thetford, H. Hagen, E. E. Stangland, J. M. Moulijn, S. H. Taylor, D. J. Willock, and G. J. Hutchings, *ACS Catalysis*, 2013, **3**(8), 1835–1844.

[31] C. Kalamaras, D. Palomas, R. Bos, A. Horton, M. Crimmin, and K. Hellgardt, *Catalysis Letters*, 2016, **146**(2), 483–492.

[32] M. H. Groothaert, P. J. Smeets, B. F. Sels, P. A. Jacobs, Schoonheydt, and R. A., *Journal of American Chemical Society*, 2005, **127**, 1394–1395.

[33] P. J. Smeets, M. H. Groothaert, and R. A. Schoonheydt, *Catalysis Today*, 2005, **110**(3-4), 303–309.

[34] N. V. Beznis, B. M. Weckhuysen, and J. H. Bitter, *Catalysis Letters*, 2010, **138**(1-2), 14–22.

[35] K. Narsimhan, V. K. Michaelis, G. Mathies, W. R. Gunther, R. G. Griffin, and Y. Román-Leshkov, *Journal of the American Chemical Society*, 2015, **137**(5), 1825–1832.

[36] T. Sheppard, H. Daly, A. Goguet, and J. M. Thompson, *ChemCatChem*, 2016, **8**(3), 562–570.

[37] E. M. C. Alayon, M. Nachtegaal, A. Bodi, and J. A. van Bokhoven, *ACS Catalysis*, 2014, **4**(1), 16–22.

[38] S. Grundner, M. A. C. Markovits, G. Li, M. Tromp, E. A. Pidko, E. J. M. Hensen, A. Jentys, M. Sanchez-Sanchez, and J. A. Lercher, *Nature Communications*, 2015, **6**, 7546.

[39] M. J. Wulfers, S. Teketel, B. Ipek, and R. F. Lobo, *Chemical Communications*, 2015, **51**(21), 4447–4450.

[40] V. Sobolev, K. Dubkov, O. Panna, and G. Panov, *Catalysis Today*, 1995, **24**, 251–252.

[41] G. Panov, V. Sobolev, K. Dubkov, V. Parmon, N. Ovanesyan, A. Shilov, and A. Shteinman, *Reaction Kinetics and Catalysis Letters*, 1997, **61**(2), 251–258.

[42] P. Knops-Gerrits and W. G. III, *Journal of Molecular Catalysis A: Chemical*, 2001, **166**, 135–145.

[43] E. V. Starokon, M. V. Parfenov, L. V. Pirutko, S. I. Abornev, and G. I. Panov, *The Journal of Physical Chemistry C*, 2011, **115**(5), 2155–2161.

[44] M. V. Parfenov, E. V. Starokon, L. V. Pirutko, and G. I. Panov, *Journal of Catalysis*, 2014, **318**, 14–21.

[45] N. V. Beznis, B. M. Weckhuysen, and J. H. Bitter, *Catalysis Letters*, 2009, **136**(1-2), 52–56.

[46] M. C. Kung, S. S. Y. Lin, and H. H. Kung, *Topics in Catalysis*, 2012, **55**(1-2), 108–115.

[47] Y. K. Krisnandi, B. A. P. Putra, M. Bahtiar, Zahara, I. Abdullah, and R. F. Howe, *Procedia Chemistry*, 2015, **14**, 508–515.

[48] T. Sheppard, C. D. Hamill, A. Goguet, D. W. Rooney, and J. M. Thompson, *Chemical Communications*, 2014, **50**(75), 11053–5.

[49] K. Narsimhan, K. Iyoki, K. Dinh, and Y. Roman-Leshkov, *ACS Central Science*, 2016, **2**(6), 424–9.

[50] P. Tomkins, A. Mansouri, S. E. Bozbag, F. Krumeich, M. B. Park, E. M. Alayon, M. Ranocchiari, and J. A. van Bokhoven, *Angewandte Chemie International Edition*, 2016, **55**(18), 5467–71.

[51] C. E. Taylor and R. P. Noceti, *Catalysis Today*, 2000, **55**, 259–267.

[52] C. E. Taylor, *Catalysis Today*, 2003, **84**(1-2), 9–15.

[53] Y. Hu, Y. Nagai, D. Rahmawaty, C. Wei, and M. Anpo, *Catalysis Letters*, 2008, **124**(1-2), 80–84.

[54] S. Impeng, P. Khongpracha, C. Warakulwit, B. Jansang, J. Sirijaraensre, M. Ehara, and J. Limtrakul, *RSC Advances*, 2014, **4**(24), 12572.

[55] F. M. Aghamir, N. S. Matin, A. H. Jalili, M. H. Esfarayeni, M. A. Khodagholi, and R. Ahmadi, *Plasma Sources Science and Technology*, 2004, **13**(4), 707–711.

[56] A. Indarto, J.-W. Cho, H. Lee, H. K. Song, and J. Palgunadi, *Journal of Rare Earths*, 2006, **24**(5), 513–518.

[57] A. Indarto, *IEEE Transactions on Dielectrics and Electrical Insulation*, 2008, **15**(4), 1038–1043.

[58] J. S. Woertink, P. J. Smeets, M. H. Groothaert, M. A. Vance, B. F. Sels, R. A. Schoonheydt, and E. I. Solomon, *Proceedings of the National Academy of Sciences*, 2009, **106**(45), 18908–18913.

[59] A. R. Kulkarni, Z.-J. Zhao, S. Siahrostami, J. K. Nørskov, and F. Studt, *ACS Catalysis*, 2016, pp. 6531–6536.

[60] E. M. C. Alayon, M. Nachtegaal, A. Bodi, M. Ranocchiari, and J. A. van Bokhoven, *Physical Chemistry Chemical Physics*, 2015, **17**(12), 7681–7693.

[61] K. Yoshizawa, Y. Shiota, T. Yumura, and T. Yamabe, *Journal of Physical Chemistry*, 2000, **104**(734-740).

[62] B. Michalkiewicz, *Applied Catalysis A: General*, 2004, **277**(1-2), 147–153.

[63] S. Pabchanda, P. Pantu, and J. Limtrakul, *Journal of Molecular Catalysis A: Chemical*, 2005, **239**(1-2), 103–110.

[64] B. R. Wood, J. A. Reimer, A. T. Bell, M. T. Janicke, and K. C. Ott, *Journal of Catalysis*, 2004, **225**(2), 300–306.

[65] E. V. Starokon, M. V. Parfenov, S. S. Arzumanov, L. V. Pirutko, A. G. Stepanov, and G. I. Panov, *Journal of Catalysis*, 2013, **300**, 47–54.

[66] N. V. Beznis, A. N. C. van Laak, B. M. Weckhuysen, and J. H. Bitter, *Microporous and Mesoporous Materials*, 2011, **138**(1-3), 176–183.

[67] P. Tang, Q. Zhu, Z. Wu, and D. Ma, *Energy & Environmental Science*, 2014, **7**(8), 2580.

[68] B. Ipek and R. F. Lobo, *Chem Commun (Camb)*, 2016, **52**(91), 13401–13404.

[69] W. L. Bragg, *Proceedings of the Royal Society of London. Series A, Containing Papers of a Mathematical and Physical Character.*, 1913, **89**(610), 248–277.

[70] P. Scherrer, *Nachrichten von der Gesellschaft der Wissenschaften zu Göttingen, Mathematisch-Physikalische Klasse*, 1918, pp. 98–100.

[71] S. Brunauer, P. H. Emmett, and E. Teller, *Journal of the American Chemical Society*, 1938, **60**, 309–319.

[72] J. Nilsson, P. A. Carlsson, S. Fouladvand, N. M. Martin, J. Gustafson, M. A. Newton, E. Lundgren, H. Gronbeck, and M. Skoglundh, *Acs Catalysis*, 2015, **5**(4), 2481–2489.

[73] E. Becker, P. A. Carlsson, L. Kylhammar, M. A. Newton, and M. Skoglundh, *Journal of Physical Chemistry C*, 2011, **115**(4), 944–951.

[74] G. Lapisardi, L. Urfels, P. Gelin, M. Primet, A. Kaddouri, E. Garbowski, S. Toppi, and E. Tena, *Catalysis Today*, 2006, **117**(4), 564–568.

[75] E. Garbowski, C. Feumijantou, N. Mouaddib, and M. Primet, *Applied Catalysis a-General*, 1994, **109**(2), 277–291.

[76] *International Zeolite Association Webpage*, **http://europe.iza-structure.org**.

[77] C. Lamberti, S. Bordiga, M. Salvalaggio, G. Spoto, and A. Zecchina, *Journal of physical Chemistry B*, 1997, **101**(3), 344–360.

[78] M. H. Groothaert, J. A. v. Bokhoven, A. A. Battiston, B. M. Weckhuysen, and R. A. Schoonheydt, *Journal of American Chemical Society*, 2002, **125**, 7629–7640.

[79] P. Vanelderen, R. G. Hadt, P. J. Smeets, E. I. Solomon, R. A. Schoonheydt, and B. F. Sels, *Journal of Catalysis*, 2011, **284**(2), 157–164.

[80] M.-L. Tsai, R. G. Hadt, P. Vanelderen, B. F. Sels, R. A. Schoonheydt, and E. I. Solomon, *Journal of the American Chemical Society*, 2014, **136**(9), 3522–3529.

[81] T. Yumura, Y. Hirose, T. Wakasugi, Y. Kuroda, and H. Kobayashi, *ACS Catalysis*, 2016, **6**(4), 2487–2495.

[82] G. Li, P. Vassilev, M. Sanchez-Sanchez, J. A. Lercher, E. J. M. Hensen, and E. A. Pidko, *Journal of Catalysis*, 2016, **338**, 305–312.

[83] P. J. Smeets, J. S. Woertink, B. F. Sels, E. I. Solomon, Schoonheydt, and R. A., *Iorganic Chemistry*, 2010, **49**(8), 3573–3583.

[84] S. M. Campbell, X.-Z. Jiang, and R. F. Howe, *Microporous and Mesoporous Materials*, 1999, **29**, 91–108.

Appendix

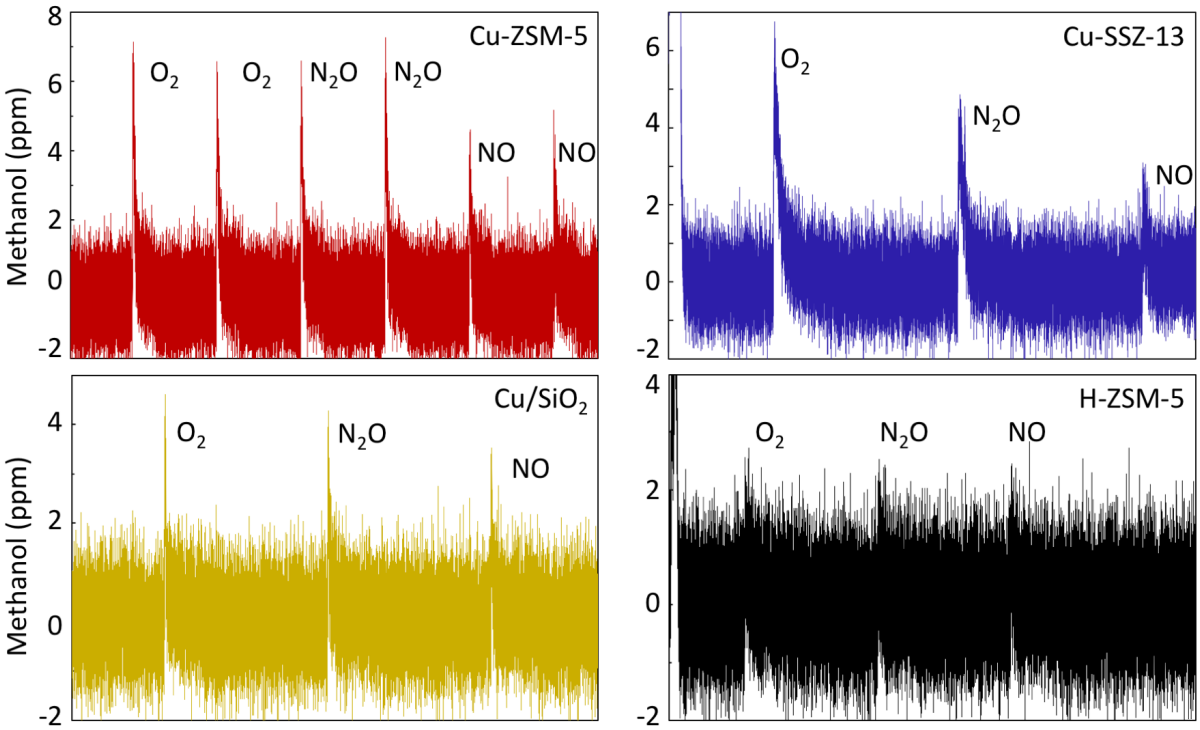

Figure A1: FTIR signal of methanol during DCMM reaction cycles. The sharp increase of methanol signal occurs while water extraction starts. Oxidants used during catalyst activation are marked as O_2, N_2O and NO.

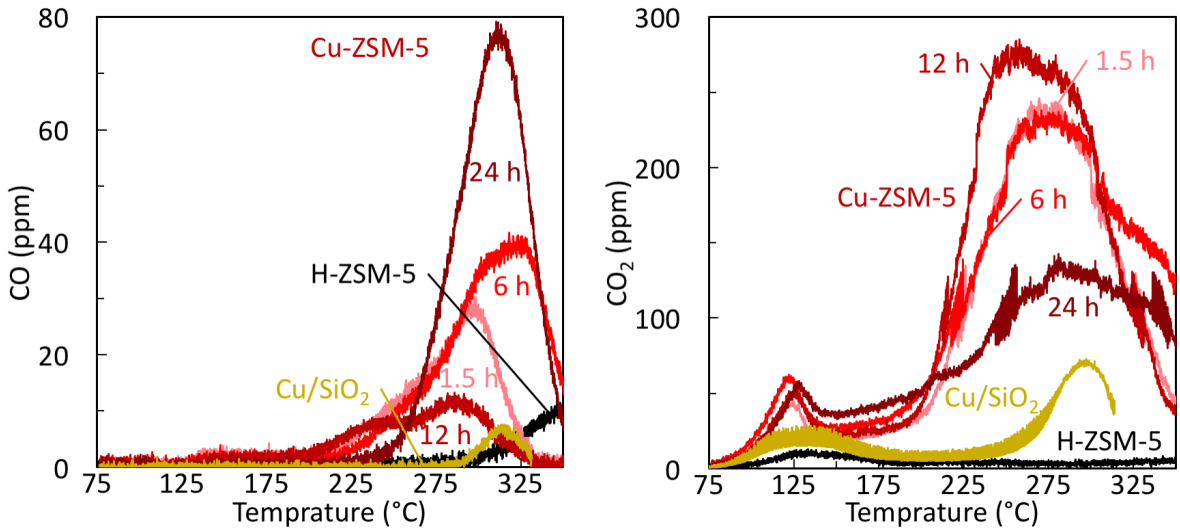

Figure A2: Desorbed gas phase species during methanol-TPD on Cu-ZSM-5, H-ZSM-5 and Cu/SiO_2. Left panel: CO; right panel: CO_2.